Physics-Based, Reduced-Order Combustor Flow Modeling

by

Sean D. Bradshaw

B.S., Aeronautics and Astronautics, Massachusetts Institute of Technology, 2000

Submitted to the Department of Aeronautics And Astronautics
in partial fulfillment of the requirements for the degree of

Master's of Science in Aeronautics And Astronautics

at the

MASSACHUSETTS INSTITUTE OF TECHNOLOGY

June 2002

Author .....
Sean D. Bradshaw
Department of Aeronautics And Astronautics
May 24, 2002

Certified by .....
David L. Darmofal
Associate Professor
Thesis Supervisor

Accepted by .....
Wallace Earl Vander Velde
Chairman, Department Committee on Graduate Students

Physics-Based, Reduced-Order Combustor Flow Modeling

by

Sean D. Bradshaw

Submitted to the Department of Aeronautics And Astronautics
on May 24, 2002, in partial fulfillment of the
requirements for the degree of
Master's of Science in Aeronautics And Astronautics

Abstract

A physics-based, reduced-order combustor flow model, CFLOW, is described which captures the essential features of physical flow phenomena characteristic of combustors. The compressible flow equations are solved on a stream-aligned grid using a Newton-Raphson method. The effects of combustor flow phenomena such as shear layers and recirculation zones are represented by simple turbulence models and semi-empirical relationships. Two turbulence modeling approaches are presented which capture the mixing processes in combustor flows. Validation studies are conducted in order to assess the merits of the proposed turbulence models.

Thesis Supervisor: David L. Darmofal
Title: Associate Professor

Acknowledgments

A wise man once said that it takes a village to raise a child. I believe that this applies to this thesis, which would not have been possible without the love and support of many people.

My advisor, Dave Darmofal, has always pushed me to be a more critical thinker. I have always been amazed by his ability to seemingly conjure up 101 different approaches to solving any one particular problem. That alone is an inspiration.

Professors Harris and Clarke have served as my mentors since day one at MIT. They have always had my best interests at heart whether I knew what they were or not. It's been an honor knowing them, working for them, and striving to be like them.

The entire ACDL/FDRL student staff deserves as much credit for this thesis as anyone. At first, I didn't know if I would fit in with this crew. But I quickly learned what a valuable asset they are. I have come to respect each and every person in the Lab. Certain people deserve honorable mention:

1. I consider David Venditti to be an intellectual giant, yet he is always humble and willing to help his fellow CFDers. I have certainly been the recipient of this help on many occasions. Thanks, Dave.

2. Joe Alescio has always tried to emulate my hairstyle. Ironically, I have always strived to emulate his diligence in the pursuit of his goals. On a more practical matter, thanks for your help in 16.920! What a class!

3. Vince Sidwell and I began our graduate tenure at MIT together in the Gas Turbine Lab., a world far, far way from our beloved ACDL. Since then, I have been impressed by his limitless excitement about being here at MIT. Combining this quality with the fact that he has actual industry experience makes him one of the more interesting people in the Lab. Vince, it's been a pleasure knowing you.

4. Victor Garzon always knows the answer to my system administration queries. Without him, nothing would work.

5. Keith Dalbey has saved CFLOW on many occasions. You haven't been cited in the thesis, but your mark is all over this work. Thanks, Keith.

6. Where would we be without Jean Sofronas? The answer is nowhere. She also provides the free food every Friday!

7. The B.O.C. (Back Office Crew), Ricardo Powell and Tony Lau, have certainly made the last few months more interesting than usual. Ricardo has been trying for months to brainwash me into thinking probabilistically. No matter, how hard he tries, I believe that the probability of leaving the lab still thinking deterministically is . . . wait a minute! Tony is the only person in the Lab. (other than myself) who actually follows the NBA! In a world of hockey fanatics, it's nice to have someone around who actually likes a sport where all of the athletes have teeth!

My family has always supported my educational pursuits. My foundation comes from my parents, who have sacrificed much to move across the Atlantic Ocean in order to live in this great country. Undoubtedly, my work ethic is derived from my Dad's example. I only hope that one day I could be as good a father as he. My Mom has always believed that her son could do whatever and be whatever he wants, by hook or crook. That's why we moved to the United States! Mommy and Daddy, for your 23 years and 11 months of support, this thesis is dedicated to you.

My brothers, Ryan and Kris, have always been my best friends. I could not imagine life without you. Thank you for your encouragement.

Finally, to my fiancée, Janelle, I owe the greatest gratitude. No one knows me and what I've been through these past 2 years more than you. Thank you for being my best friend, the voice of reason, my partner-in-crime, and letting me know that my leather jacket needs to go. I love you.

This research was supported by GEM Foundation, United Technologies, and the MIT Dean for Graduate Students.

Contents

List of Figures

Chapter 1

Introduction

1.1 Background and Motivation

Combustor flows are characterized by a wide range of physical flow phenomena which are difficult to simulate with three-dimensional, transient Computational Fluid Dynamic (CFD) simulations. Boundary layers line the pre-diffuser, diffuser, and burner walls. Two large recirculation zones occupy the dump region between the pre-diffuser exit and the burner entrance. In addition, the recirculation zones re-attachment points fluctuate with respect to time, which adds another modeling difficulty. The burner hood also introduces a region of high velocity flow with strong streamline curvature, which increases the local turbulence levels and decreases the total pressure. In addition to the difficulties presented by modeling the aforementioned phenomena, CFD packages are computationally expensive, typically requiring several hours if not days to run. As a result, engineering necessity requires that the combustor design engineer use conceptual and semi-empirical models in order to arrive at an acceptable design within the specified time limits.

CFD simulations are used near the end of the design process in order to predict phenomena that were not accounted for in the preliminary design phase. Design corrections in the latter phases of the design process, however, can lead to significant costs for engineering re-work and delays in product delivery. Hence, there is a critical need for higher fidelity simulations to be introduced into the earlier phases of the design process. CFLOW, a physics-based lower order model of combustor flows, is proposed in order to address this need. CFLOW models combustor flows essentially as compressible and inviscid with mass, momentum, and energy transfer source terms to include turbulent mixing effects. These

source terms require the bulk of the modeling effort. The reduced complexity of this lower-order model renders it less computationally expensive than high-fidelity simulations.

The basic modeling approaches used in CFLOW are based on the work of Underwood [2] and Drela [3]. Underwood sought to predict the behavior of confined swirling flows with heat addition using various reduced-order computational flow models. In one of these schemes, the flow is solved on a stream-aligned grid in order to minimize numerical dissipation. Thus, the total pressure loss is zero for smooth geometries unless loss mechanisms are added to the model. Underwood employs the empirical relationship for the growth rate of plane mixing layers presented by Dimotakis [13] in order to arrive at expressions for the transport terms.

In this thesis, two modeling approaches are presented for the effects of turbulent mixing on the mean combustor flow. The first model applies Prandtl's second hypothesis, which relates the eddy viscosity to the velocity difference across a mixing layer and the thickness, to the turbulent viscosity hypothesis developed by J. Boussinesq. Prandtl's equation is substituted into the shear stress equation, which eliminates the eddy viscosity and mixing layer thickness from the expression (see Chapter 3). The result is that the turbulent shear stress is a function of the density, the velocity difference squared, and a mixing constant determined from Dimotakis' study. The second approach (see Chapter 4) uses the Boussinesq expression explicitly, instead of substituting for eddy viscosity and the mixing layer thickness, in order to arrive at a model in which the turbulent eddy viscosity and shear layer thickness evolve with the flow. Specifically, the von Karman Integral Momentum Equation and the Spalart-Allmaras Equation [4] were chosen to represent the evolution of the eddy viscosity and mixing layer thickness. Drela [3] integrated the continuity and the axial component of the Navier-Stokes Equations for a 2D compressible thin shear layer in order to arrive at the Integral Momentum Equation for a mixing layer. Similarly, the continuity and Spalart-Allmaras (S-A) equations were integrated across the mixing layer in order to arrive at the integral form of the S-A equation used in CFLOW. Reasonable assumptions about the eddy viscosity, density, and velocity profiles were made in order to utilize this integral approach. However, calibration to the physical flow becomes a necessity as a result.

1.2 Research Objectives

The goal of the research effort is to develop an easily calibrated physics-based, reduced-order computational flow model which accurately captures the effects of shear layers and recirculation zones on critical combustor design parameters, such as total pressure loss and mass flow distribution. These metrics will then be validated against experimental results from combustor-diffuser performance studies.

1.3 Thesis Overview

Chapter 2 first describes combustor flow phenomena and terminology. The basic governing equations for compressible inviscid flow and the mass, momentum, and energy transfer terms are presented. Finally, the damped Newton solver is discussed.

Chapter 3 presents the theoretical approach and numerical results of the Algebraic Turbulent Shear-Layer Model. The plane mixing layer is introduced as the mechanism for momentum transfer between adjacent streams. Mass and energy transfer terms are assumed to be negligible compared to momentum transfer terms. In addition, the wall shear stress model is discussed briefly. Finally, the results of the algebraic model are compared to several combustor/diffuser performance studies.

In Chapter 4, the theoretical approach and numerical results of the Turbulent Integral Shear-Layer Model are presented. The governing equations are derived, calibrated, and then discretized for implementation in CFLOW. Finally, the results of this model are compared to those of the algebraic model and the combustor/diffuser performance studies.

Chapter 5 summarizes the theoretical approaches of both turbulence models, discusses the results of the validation studies, and outlines recommendations for future work on CFLOW.

Chapter 2

Combustor Flow Modeling

The purpose of this chapter is to discuss combustor flows and the foundation of the CFLOW model. First, the physical flow features as air passes through each component of the combustor are briefly discussed. Second, the streamtube model and the numerical stencil are described. Third, the mean flow governing equations and matching conditions are presented. Finally, the Newton solver is discussed.

2.1 Combustor Flows

The annular dump combustor layout has been the automatic choice for all new aircraft engines since the 1960s [5]. The CF6-50, one of the engines fitted with annular dump combustors, is shown in Figure 2-1. A typical combustor of this type consists of a prediffuser, a diffuser, a burner, a burner dome, shrouds, fuel injectors, fuel igniters, and liners. For the analysis undertaken in this thesis, this layout has been idealized in manner shown in Figure 2-2, where the fuel injectors and igniters have been omitted and the geometry has been simplified. The prediffuser accepts highly turbulent, high pressure flow from the high pressure compressor and decreases the Mach number from about 0.5 to 0.3. Further diffusion is necessary in order to reduce the total pressure losses in the dump gap; the diffuser serves this purpose. Recirculation zones present in the dump gap reduce the total pressure and increase the entropy of the gas. After diffusion, the flow splits into three branches:

1. The primary zone.

2. The area between the outer shroud diameter and the outer burner diameter.

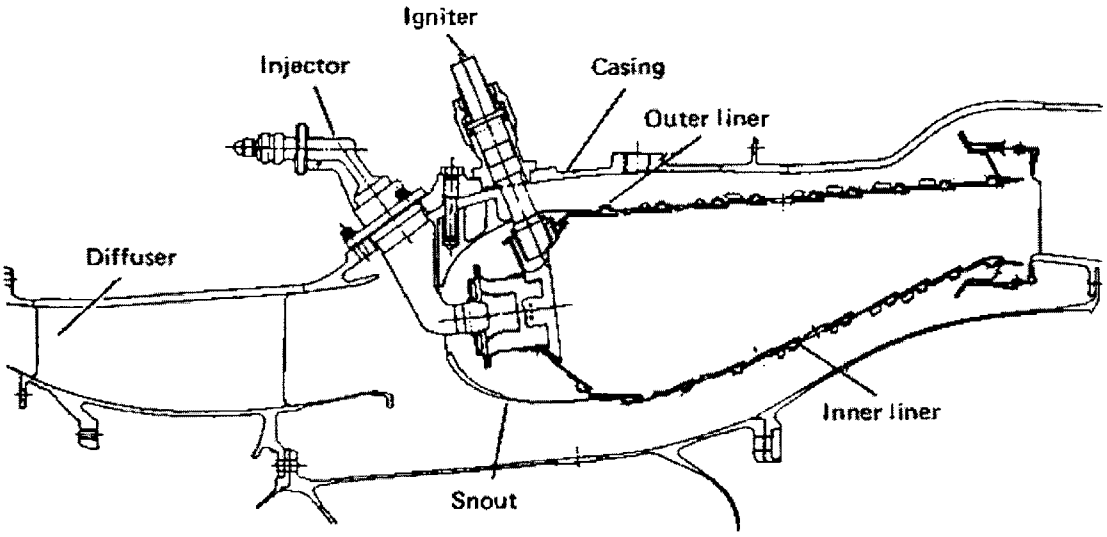

CF6-50 annular combustor (*courtesy General Electric Company*).

Figure 2-1: CF6 Cutaway

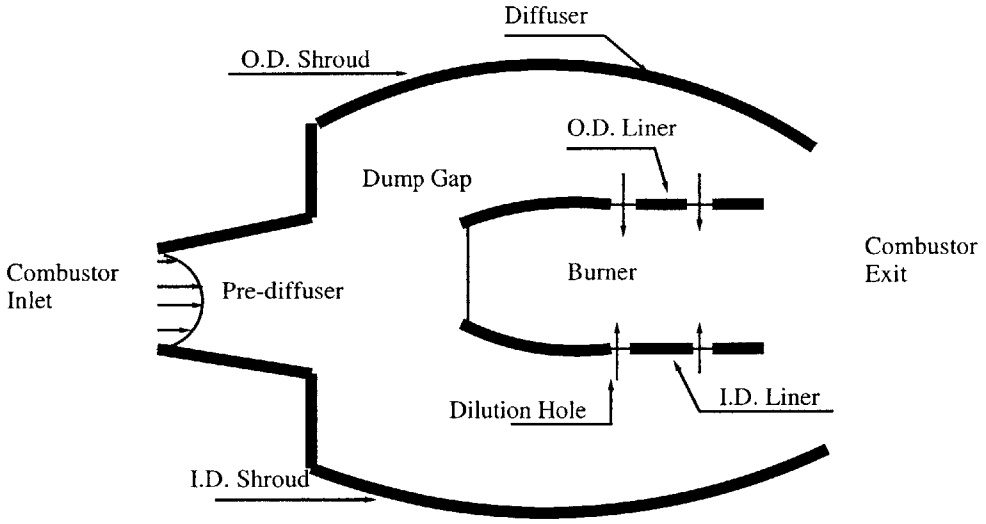

O.D. - Outer Diameter
I.D. - Inner Diameter

Figure 2-2: Combustor schematic

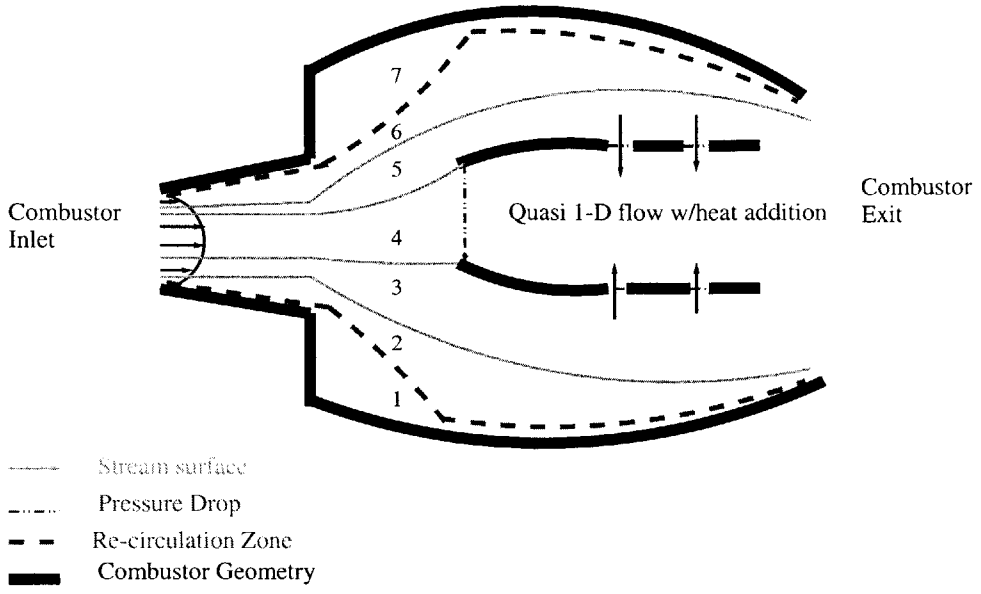

Figure 2-3: Combustor features

3. The area between the inner shroud diameter and the inner burner diameter.

This flow split insures that the equivalence ratio of the turbulent, reacting flow in the entrance of the burner primary zone is near or greater than one (depending on the power setting). Further downstream, the reaction is quenched by added air from the shroud passage flows via the dilution holes. However, this process also causes a drop in the total pressure. In addition, the process of forcing flow through the burner hood, which contains the fuel nozzles, incurs even more total pressure losses.

2.2 Streamtube Model and Stencil

The CFLOW model divides the flow into several stream tubes in order to capture the effects of the recirculation zones and the flow distribution around the burner hood separately (Figure 2-3). In the current version, seven streamtubes have been used. Streamtubes 1 and 7 are used to capture the recirculation zones in the dump gap. Streamtube 4 represents the burner mass flow. The remaining streamtubes are distributed around the dome. This approach enables the total pressure distribution at the pre-diffuser inlet to be approximated. The flow within each streamtube conserves mass, momentum, and energy unless specific mechanisms are added to the model that permit mass diffusion, momentum dissipation, heat

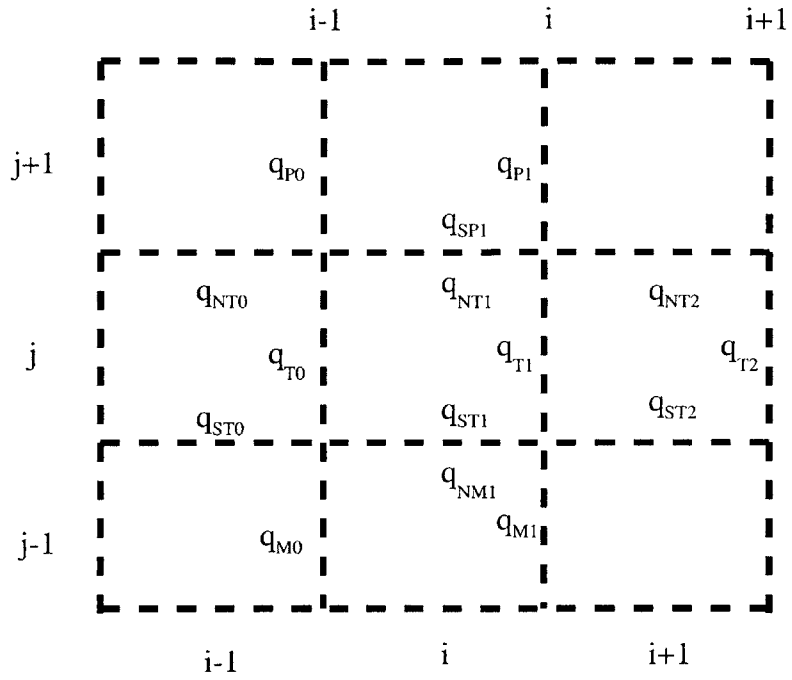

Figure 2-4: CFLOW Index Notation

transfer, and work transfer. These mechanisms are represented in the governing equations by source terms, which must be modeled. The flow is assumed to be a steady, compressible, turbulent flow that behaves like a calorically perfect gas. The governing equations that are presented in Section 2.3 model the mean quantities of the fluid mechanical variables.

The seven streamtubes and a specified number of axial grid lines form an array of control volume cells (Figure 2-4). CFLOW solves the compressible flow equations for each cell until streamsurface locations are aligned with the grid. A typical grid for a converged CFLOW simulation is shown in Figure 2-5. Each cell (i, j) contains 8 state variables and 8 equations (Figure 2-6). The axial velocity, radial velocity, density, and temperature state variables are stored on the cell faces. Pressure and the radial locations are stored on the north and south cell edges.

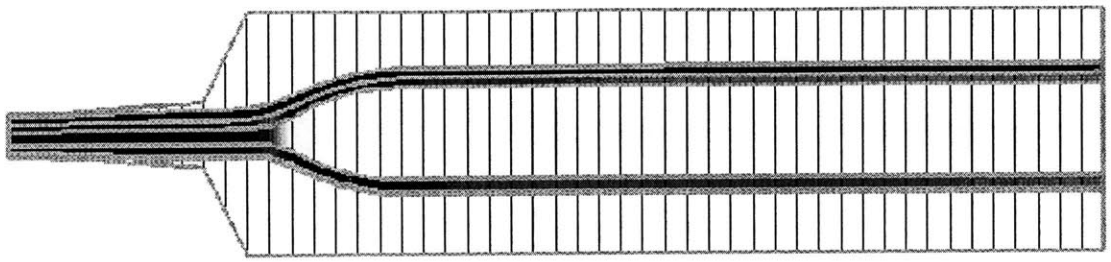

Figure 2-5: CFLOW Grid

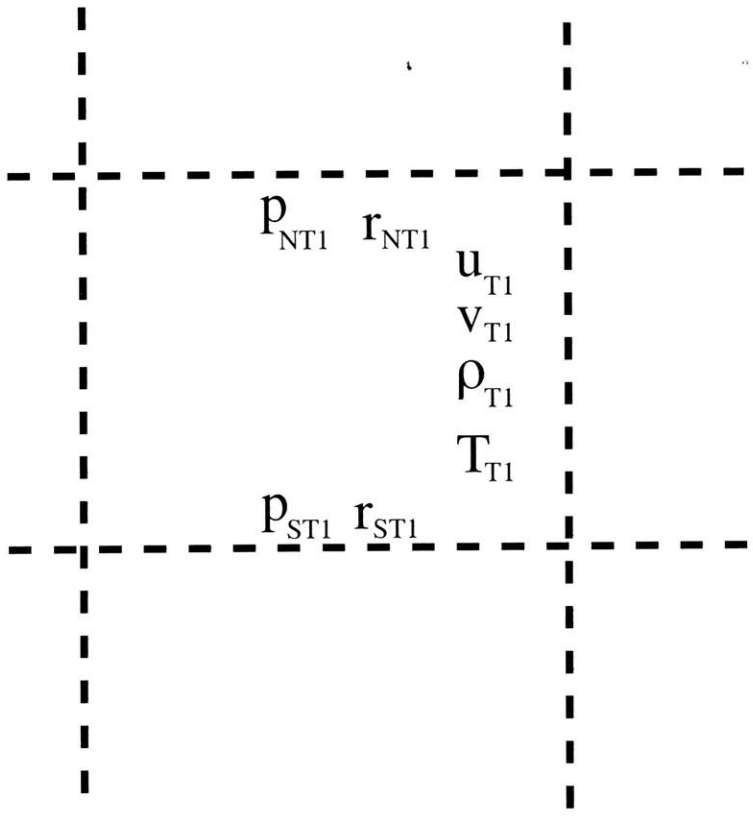

Figure 2-6: Unknowns for cell(i,j)

2.3 Main Flow Governing Equations

2.3.1 Conservation of Mass

The conservation of mass for cell(i, j) is

$$\rho_{T1} u_{T1} A_{T1} - \rho_{T0} u_{T0} A_{T0} = \tilde{M}_{PT} - \tilde{M}_{TM} \tag{2.1}$$

where ρ is the density, u is the axial velocity, and A is the cell face area. $\tilde{M}$ denotes the mass flow rate across the control volume edges as a result of turbulent mixing. Expressions for the mass transfer terms are presented in Chapters 3 and 4.

The cell faces areas are defined

$$A_{T0} = \frac{\pi}{4}[(r_{NT0} + r_{NT1})^2 - (r_{ST0} + r_{ST1})^2] \tag{2.2}$$

$$A_{T1} = \frac{\pi}{4}[(r_{NT1} + r_{NT2})^2 - (r_{ST1} + r_{ST2})^2] \tag{2.3}$$

2.3.2 Equation of Motion: Axial

The axial component of the equation of motion is

$$\rho_{T1} u_{T1}^2 A_{T1} - \rho_{T0} u_{T0}^2 A_{T0} + p_{T1} A_{T1} - p_{T0} A_{T0} + p_{ST1} \Delta A_S - p_{NT1} \Delta A_N = S_x + S_{cx}, \tag{2.4}$$

where S_x is the shear force due to the Reynolds stress and S_{cx} is the convective momentum transfer term due to turbulent mixing. The development and presentation of the expressions for S_x and S_{cx} are presented Chapters 3 and 4. ΔA_S and ΔA_N are the area changes over which the pressures on the cell edges act. They are computed by

$$\Delta A_N = \frac{\pi}{4}[(r_{NT1} + r_{NT2})^2 - (r_{NT0} + r_{NT1})^2] \tag{2.5}$$

$$\Delta A_N = \frac{\pi}{4}[(r_{ST1} + r_{ST2})^2 - (r_{ST0} + r_{ST1})^2] \tag{2.6}$$

2.3.3 Equation of Motion: Radial

The radial component of the equation of motion is

$$\rho_{T1}u_{T1}v_{T1}A_{T1} - \rho_{T0}u_{T0}v_{T0}A_{T0} - 0.5(p_{NT1} - p_{ST1})(A_S + A_N) = S_r + S_{cr} \tag{2.7}$$

where the v is the radial velocity, S_r is the radial component of the shear force acting on the control volume, and S_{cr} is the convective momentum transfer term due to turbulent mixing. The expressions for S_r and S_{cr} are presented in Chapters 3 and 4.

2.3.4 Conservation of Energy

The Conservation of Energy for a steady-state, steady flow process through cell(i, j) is

$$\rho_{T1}u_{T1}A_{T1}H_{TT1} - \rho_{T0}u_{T0}A_{T0}H_{TT0} = H_s + H_{tx} - W_s \tag{2.8}$$

where H_T is the total enthalpy, H_s is the heat transfer rate across cell(i, j), H_{tx} is the rate of enthalpy flux across cell(i, j) due to mixing, and W_s is the rate of work transfer due to shear. The expressions for the source terms are presented in Chapters 3 and 4.

2.3.5 Equation of State

The Equation of State, which ensures that the pressures on the cell faces are consistent with those on the cell edges, is

$$\rho_{T0}R_{gas}T_{T0} + \rho_{T1}R_{gas}T_{T1} - (p_{ST1} + p_{NT1}) = PSD \tag{2.9}$$

R_{gas} is the ideal gas constant for air, and T is the static temperature. PSD is a stabilization term that eliminates the pressure-streamsurface decoupling mode that occurs as the system is being updated. This term is defined in the following manner.

$$PSD = (PEPS)(\frac{1}{8}(\rho_{T0} + \rho_{T1})(u_{T0}^2 + u_{T1}^2)/A_{st1})(A_{st1} - \frac{1}{4}(A_{st0} + 2A_{st1} + A_{st2}) \tag{2.10}$$

$$A_{st0} = \pi(r_{NT0}^2 - r_{ST0}^2) \tag{2.11}$$

$$A_{st1} = \pi(r_{NT1}^2 - r_{ST1}^2) \tag{2.12}$$

$$A_{st2} = \pi(r_{NT2}^2 - r_{ST1}^2) \tag{2.13}$$

$$PEPS = 0.300 \tag{2.14}$$

2.3.6 Flow Tangency

The flow tangency condition is

$$u\frac{dr}{dx} - v = E_n \tag{2.15}$$

where E_n, the net entrainment velocity, is defined in Chapters 3 and 4. In a case where there is no mixing, $E_n = 0$ and the velocity vector is parallel to the streamline direction.

2.3.7 Matching Conditions: North and South Edges

For cells in which both edges are shear layers (as opposed to a fixed wall), the matching conditions on the north and south edges of cell(i, j) are

$$p_{NT1} = p_{SP1} \tag{2.16}$$

and

$$r_{ST1} = r_{NM1} \tag{2.17}$$

If the northern edge of cell(i, j) is a wall at a fixed radial location R_{bn}, then Equation 2.16 is replaced by

$$r_{NT1} = R_{bn} \tag{2.18}$$

If the southern edge of cell(i, j) is a wall at a fixed radial location R_{sn} then Equation 2.17 is replaced by

$$r_{ST1} = R_{sn} \tag{2.19}$$

2.4 Boundary Conditions

2.4.1 Inlet Boundary Conditions

Dirichlet boundary conditions are set at the inlet for the axial velocity, density, temperature, and both edge static pressures. The radial velocity is determined by the flow tangency condition. The radial locations corresponding to the northern edge of streamtube 7, the southern edge of streamtube 1, and both edges of streamtubes 2 and 6 are fixed. Neumann conditions apply to the streamsurfaces which emanate from the lip of the dome walls (see Figure 2-3). This condition allows these streamsurfaces to float until the prescribed burner mass flow rate is achieved.

2.4.2 Outlet Boundary Conditions

Dummy Dirichlet boundary conditions are applied to all fluid mechanical state variables at the outlet. Neumann boundary conditions are set for northern and southern streamsurfaces locations corresponding to streamtubes 2 and 6. The other 4 streamsurfaces are fixed to the prescribed combustor geometry via Dirichlet conditions.

2.5 Newton-Raphson Solver

The system of nonlinear model equations is setup and solved simultaneously using a damped Newton-Raphson method. The equations and state variables are stored in the residual vector, R, and the state vector, Q, respectively. The goal is to find the state vector, Q_*, which satisfies Equation 2.20.

$$R(Q_*) = 0 \tag{2.20}$$

In order to do so, R is linearized about Q at iteration i, as shown in Equation 2.21 and Equation 2.22. $\frac{\partial R}{\partial Q}$ is the Jacobian matrix, which contains the partial derivatives of the governing equations with respect to the state variables,

$$R(Q_i + \Delta Q_i) = 0 \tag{2.21}$$

$$R(Q_i) + \frac{\partial R}{\partial Q}\Delta Q_i \approx 0 \tag{2.22}$$

$$\frac{\partial R}{\partial Q}\Delta Q_i \approx -R(Q_i) \tag{2.23}$$

$$Q_{i+1} = Q_i + \omega_i \Delta Q_i \tag{2.24}$$

ΔQ_i is solved in Equation 2.23 using a tri-diagonal block solver. The state vector is updated in Equation 2.24, where ω_i is the relaxation parameter at each iteration. For the all state variables except the radial velocity, the relaxation parameter is determined in the following manner:

$$\omega_i = \begin{cases} \frac{kQ_i}{|\Delta Q_i|} & : \mid \Delta Q_i \mid > kQ_i \\ 1 & : \mid \Delta Q_i \mid \leq kQ_i \end{cases}$$

For the radial velocity,

$$\omega_i = \begin{cases} \frac{k}{|\Delta Q_i|} & : \mid \Delta Q_i \mid > k \\ 1 & : \mid \Delta Q_i \mid \leq k \end{cases}$$

In this damping scheme, $k \sim 0.1$. The minimum value of the relaxation parameter is chosen for the newton update. This damping scheme is used to prevent the state variables, except the radial velocity, from becoming negative during the newton updates. For example, a negative value of pressure is not permissible in CFLOW. However, negative values of radial velocity are physically possible. This procedure continues until the l_2-norm of R is below 10^{-10}. The initial state vector, Q_0, must be relatively close to Q_* in order for the system to converge. Thus, Q_0 is specified based on the inlet conditions (for the fluid mechanical variables) and local geometry (for the radial locations of the streamlines).

Chapter 3

Algebraic Turbulent Shear Layer Model

The purpose of this chapter is to introduce the Algebraic Turbulent Shear Layer Model. First, the bases for the momentum tranport mechanism used in CFLOW are explained. Then, the modeling assumptions are stated and an algebraic turbulent shear layer model is derived. Finally, this chapter concludes with a validation study, where critical combustor performance metrics are studied.

3.1 Theoretical Approach

Turbulent flow over a backward facing step is similar to the flow leaving the pre-diffuser and entering the dump gap. The thin boundary layers on the pre-diffuser walls separate, curve sharply toward the diffuser walls, and then re-attach. The actual re-attachment point is a function of time [14]. The region between the diffuser wall and the shear layer is called the recirculation zone. Large eddies on the order of the step height pass through the re-attachment region. Baker [16], Eaton and Johnson [15], and McGuiness [17] computed the growth rates of reattaching shear layers and compared them to the growth rates of plane mixing layers. It was found that reattaching shear layer growth rate was comparable to the plane mixing layer growth rate. In addition, the mean velocity profiles were identical in the outer three-fourths of the layer. The difference is found in the region near the low-speed edge, where the turbulence intensity is higher for the reattaching shear layer case compared to the plane mixing layer case. Eaton concluded that the reattaching shear layer is similar

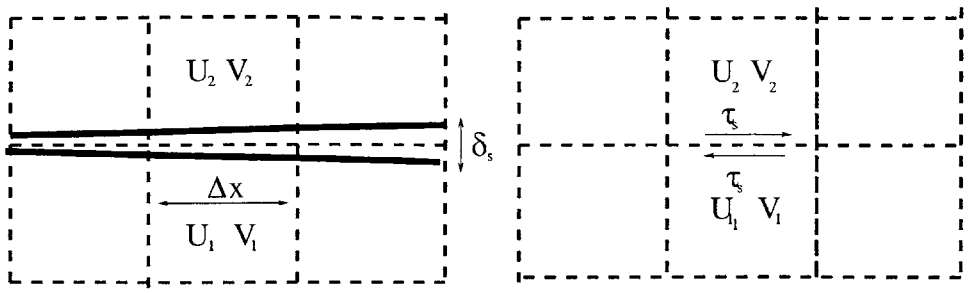

Figure 3-1: CFLOW mixing layer

to a plane-mixing layer upstream of the reattaching zone.

The CFLOW algebraic turbulence model uses the plane mixing layer as the principal mechanism for momentum transfer between streams. Based on the work of Eaton, it is appropriate to use the plane mixing layer to model the turbulent interactions between the mean flow and the recirculation zone in the dump gap. For simplicity, the model is used in the pre-diffuser region and the diffuser regions that are downstream of the dump gap to facilitate mixing between adjacent streams with differing velocities.

The first approach to the turbulent mixing layer model consists of the following assumptions:

1. The mixing layer is thin ($\frac{\delta}{L} \ll 1$), where L is a physical axial length scale, like the length of the combustor.

2. The flow is highly turbulent ($\frac{\nu_t}{\nu} \gg 1$).

3. Tangential velocity difference across mixing layer is small ($\frac{\Delta U}{U_{ave}} \ll 1$).

4. Pressure gradients are negligible compared to viscous diffusion.

5. Streamline curvature effects are negligible.

6. Mass and energy transfer are negligible, and their source terms are set to zero in CFLOW.

7. Compressibility effects are negligible; the mixing layer is incompressible.

The mass flow rate of air through the mixing layer is negligible compared to the mass flow rate across the cell faces as a result. Therefore, the effect of the mixing layer on

the mean flow are represented by shear stresses on the cell edges in this turbulence model (Figure 3-1). In addition, convection and diffusion through the shear layer are neglected.

According J. Boussinesq [1], the shear stress for simple turbulent shear flows can be represented by

$$\tau_s = \rho(\nu + \nu_t)\frac{\partial u}{\partial y} \tag{3.1}$$

where ν is the kinematic viscosity, ν_t is the eddy viscosity, and u is the mean axial velocity in the mixing layer. Equation 3.1 is accurate when the turbulence characteristics and mean velocity gradients change slowly relative to the mean flow. This is the case for simple, turbulent shear flows such as the plane mixing layer. Thus, the local velocity gradients characterize the Reynolds stresses [8].

Combustor flows are highly turbulent flows where the eddy viscosity is 2 or 3 orders of magnitude larger the kinematic viscosity. Thus, the shear stress can be approximated as:

$$\tau_s = \rho\nu_t\frac{\partial u}{\partial y} \tag{3.2}$$

In addition, the flow Mach number in most of the regions downstream of the pre-diffuser is less than 0.3. Thus, the assumption of incompressibility for the mixing layer is not grossly inaccurate.

For a free mixing layer, Prandtl's second hypothesis states that the eddy viscosity is proportional to the velocity difference across two streams and the layer thickness. Hence,

$$\nu_t = K_\nu \Delta U \delta \tag{3.3}$$

where K_ν is an empirical constant. In CFLOW, K_ν is calibrated based on values determined for plane mixing layers. The rule of thumb for such flows is: $K_\nu \sim 0.01$. Combining the Boussinesq analogy and Prandtl's second hypothesis with the assumption that $\frac{\partial u}{\partial y} \approx \frac{\Delta u}{\delta}$, the mixing layer Reynolds stress is

$$\tau_s = K_t \rho (\Delta U)^2. \tag{3.4}$$

Görtler (1942) [1] solved for the velocity profile of a turbulent incompressible temporal plane

mixing layer formed by two parallel streams with velocities U_1 and U_2,

$$\frac{u - U_1}{U_2 - U_1} = \frac{1}{2}[1 + erf(\frac{\sigma y}{x})] \tag{3.5}$$

where u is the mean tangential velocity within the shear layer and σ is an empirical constant. For a highly turbulent shear layer without pressure gradients and where changes in the normal direction to the flow dominate over changes in the axial direction, it can be shown from dimensional analysis (see Appendix C) that

$$\delta = K_\delta \frac{\Delta U}{U_{ave}} x \tag{3.6}$$

where K_δ is a constant determined from experiment. The linear growth of the mixing layer thickness was verified by Dimotakis [13]. Combining this result for δ and Prandtl's second hypthosis for ν_t yields

$$\nu_t = K_\nu K_\delta \frac{(\Delta U)^2}{U_{ave}} x \tag{3.7}$$

Taking the gradient of the velocity profile, evaluating it at the centerline, and substituting Equation 3.6 and Equation 3.7 into Equation 3.2 yields

$$\tau_s = 0.13\rho(\Delta U)^2 \tag{3.8}$$

Thus, in order to calibrate the shear layer model to the physical plane mixing layer case state above, K_t is set to 0.13. This analysis also shows that K_t is an empirical constant. In practice, K_t is calibrated in order to minimize the error between the performance metrics (i.e. total pressure loss) in CFLOW and in experiment.

3.2 Wall Shear Stress

The wall shear stress τ_w is represented by

$$\tau_w = C_f \frac{1}{2} \rho U^2 \tag{3.9}$$

where the turbulent skin friction coefficient, C_f, is prescribed a value typical of turbulent flows in circular pipes at Reynolds numbers characteristic of combustor flows and U is the

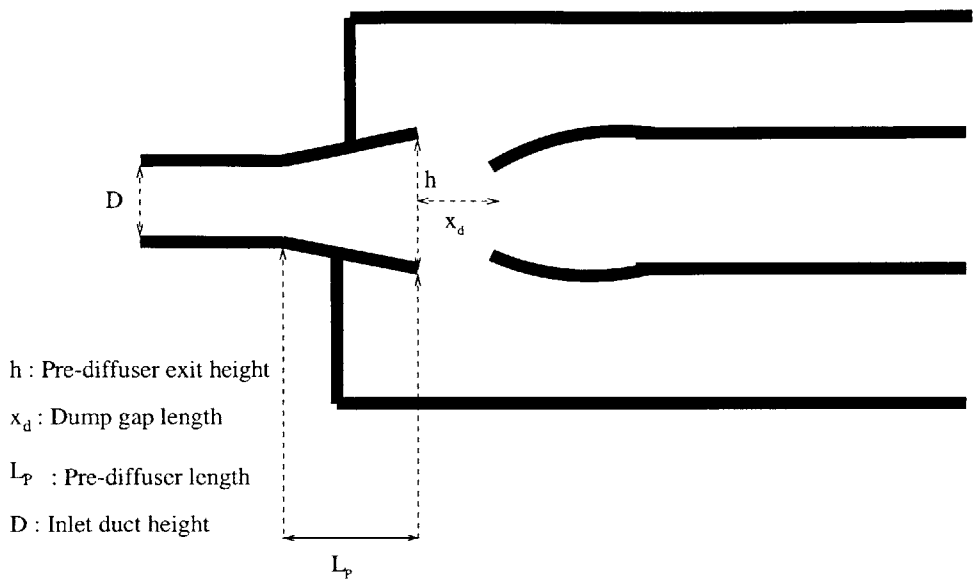

Figure 3-2: Annular Combustor/Diffuser Rig

tangential velocity of the streams which are adjacent to the combustor walls.

A nominal value is set based on the following formula by Colebrook [1].

$$\frac{1}{4C_f} \approx -2.0 \log_{10}\left(\frac{k/D}{3.7} + \frac{2.51}{Re_D\sqrt{4C_f}}\right) \tag{3.10}$$

In practice, C_f is a calibration constant in a similar manner to K_t.

3.3 Results

Lohmann et al [12] and Srinivasan et al [10] engaged in an experimental test programs which sought to investigate the aerodynamic characteristics of dump diffuser/annular burner systems in a blockage free environment (i.e. struts and fuel injector supports are absent). A schematic of these combustor/diffuser rigs is shown in Figure 3-2. The static pressure recovery, total pressure loss, and mass flow distribution measurements were collected as a function of dump gap length. This thesis focuses on the effects dump gap length on the pre-diffuser pressure recovery, the overall diffuser pressure recovery, and the diffuser total pressure loss (dump loss).

Lohmann et al found that decreasing the dump gap length causes a back pressuring of the pre-diffuser, which results in increased static pressure recovery and decreased total

pressure loss. Srinivasan et al stated that decreasing the dump gap length results in lower overall static pressure recovery and higher overall total pressure loss. These effects are due to high velocities at increased streamline curvature near the dome walls. Lohmann et al also discovered that an optimum dump gap length exists, where the overall diffuser pressure recovery is maximum. Most of the pressure recovery occurs in the pre-diffuser, while most of the total pressure loss is a result of the turbulent mixing in the dump region and around the dome.

The nominal test conditions of Lohmann et al's experiment were the following:

1. The mean inlet Mach number is 0.33.

2. The inlet Reynolds number is 300,000.

3. The inlet velocity profile is flat (as opposed to profiles with distorted velocity distributions).

4. $\frac{L_p}{D} = 4$ (see Figure 3-2)

5. No mass transfer from shrouds to burner via dilution holes.

6. Percent Mass flow split: ID(29), OD(43), primary zone(28)

CFLOW was calibrated at a dump gap ratio, x_d/D, of 1.43 in order to closely match the values given in the Lohmann experiment for pre-diffuser static pressure recovery, $C_{p_{12}}$, mass-averaged overall diffuser pressure recovery, $C_{p_{13}}$, and the mass-averaged dump loss, $C_{L_{13}}$. The CFLOW calibration constants for this study were $C_f = 0.025$ and $K_t = 0.13$. In order to simulate the flat profile case in the Lohmann experiment, the core flow (streamtubes 3, 4, and 5) Mach number was set to 0.33, and the blockage flow (streamtubes 1,2,6, and 7) Mach number was set to 0.32 (see Appendix A).

3.3.1 Flow Plots

The CFLOW results for the Lohmann study at $x_d/D = 1.43$ are shown in the following flow plots.

Mach Number

Figure 3-3 shows the Mach number distribution within the combustor rig. Streamtubes 1 and 7 are thin in the pre-diffuser. Then, they grow in the dump region as the speeds within these streams sharply decrease. The recirculation zones induce large velocity differences between streamtubes 1 and 2 and streamtubes 6 and 7, which result in increased mixing. It is important to note that in the CFLOW, there is actually no recirculating air in the dump region. This would require negative axial velocities, which are not permissible in this model. However, representing the recirculation zone as a dead air or low velocity region induces the desired effect.

Static Pressure Recovery

Figure 3-4 shows the static pressure recovery. The pre-diffuser induces most of the static pressure recovery. The radial pressure distribution becomes uniform at the combustor exit as a result of turbulent mixing.

Total Pressure Loss

Figure 3-5 demonstrates that most of the total pressure loss occurs in the dump region. The loss coefficient is aproximately 0.6 in the recirculation zones. In the core streams, C_L is approximately 0.1. Further downstream along the ID and OD flow paths, the loss coefficients of each stream approach 0.42 due to turbulent mixing.

3.3.2 Validation

Following the calibration procedure, a parametric study involving the aforementioned performance metrics was performed in order to determine CFLOW's level of modeling accuracy. In the following figures, the performance metrics for CFLOW and the Lohmann study are denoted with the suffixes 'n' and 'exp', respectively.

Pre-diffuser Static Pressure Recovery

Figure 3-6 shows that the pre-diffuser static pressure recovery predicted by CFLOW closely matches the experimental data. The maximum error between the two curves is approximately 2 percent. In addition, CFLOW captures the general trend for this metric. As

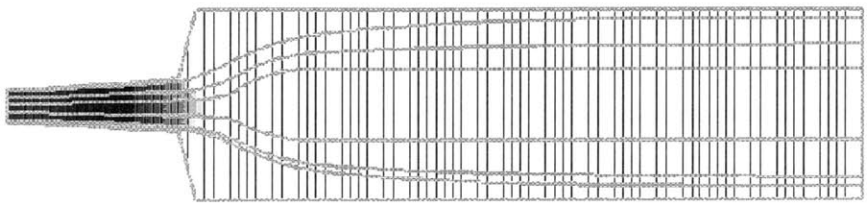

Figure 3-3: Flow Plot: Mach Number

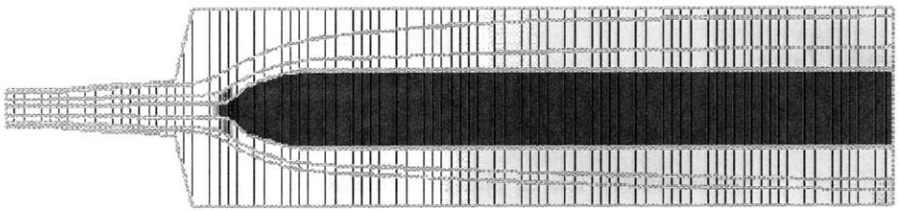

Figure 3-4: Flow Plot: Static Pressure Recovery

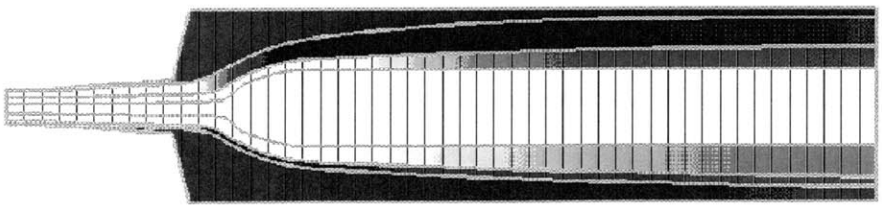

Figure 3-5: Flow Plot: Total Pressure Loss

the cowl moves closer to the pre-diffuser, there is a slight back-pressuring effect, which is represented as an increase in $C_{p_{12}}$ as x_d/D decreases.

Overall Diffuser Static Pressure Recovery

The overall diffuser static pressure recovery predicted by CFLOW matches the experimental data as well (Figure 3-7). In CFLOW, $C_{p_{13}}$ decreases as the dump gap length increases. In addition, the error between the values of the two curves is less than 4 percent. Because the margin of error of the pressure measurements was only 4 to 8 percent of their magnitudes, the error between the two curves is insignificant.

Overall Total Pressure Loss

Figure 3-5 shows that the C_L varies from stream to stream. In order to compute $C_{L_{13}}$ in CFLOW, mass-averaged measurements were taken at the combustor exit. As the Lohmann data illustrates (Figure 3-8), the dump loss is constant as the dump gap length increases from 0.43 to 2.0, then it slightly increases as x_d/D further rises. The dump loss predicted by CFLOW is roughly constant over a range of dump gap lengths. The CFLOW results do not approximate the moderate increase in the dump loss with increase dump gap length. In addition, CFLOW overpredicts the dump loss by as much as 30 percent.

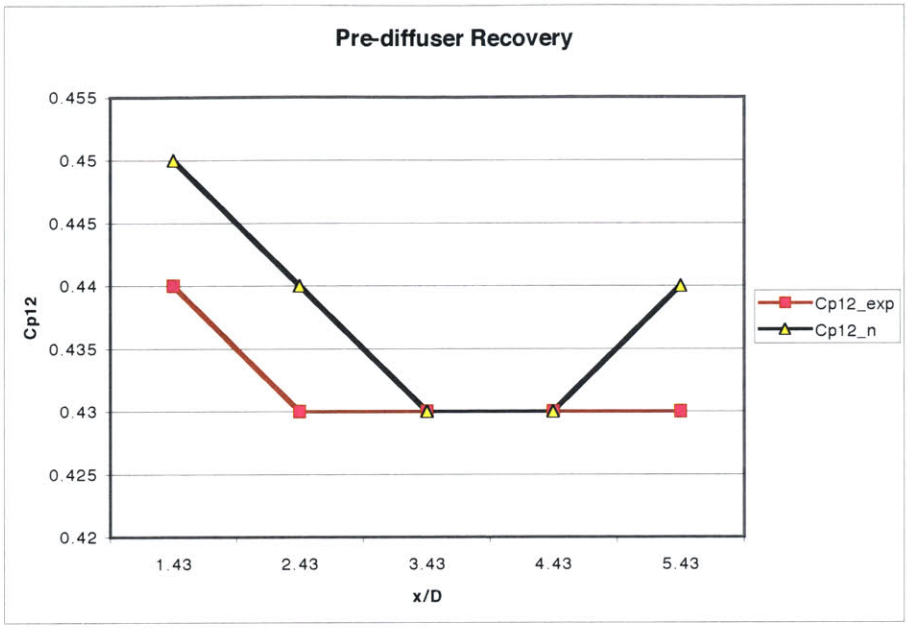

Figure 3-6: Pre-diffuser Static Pressure Recovery

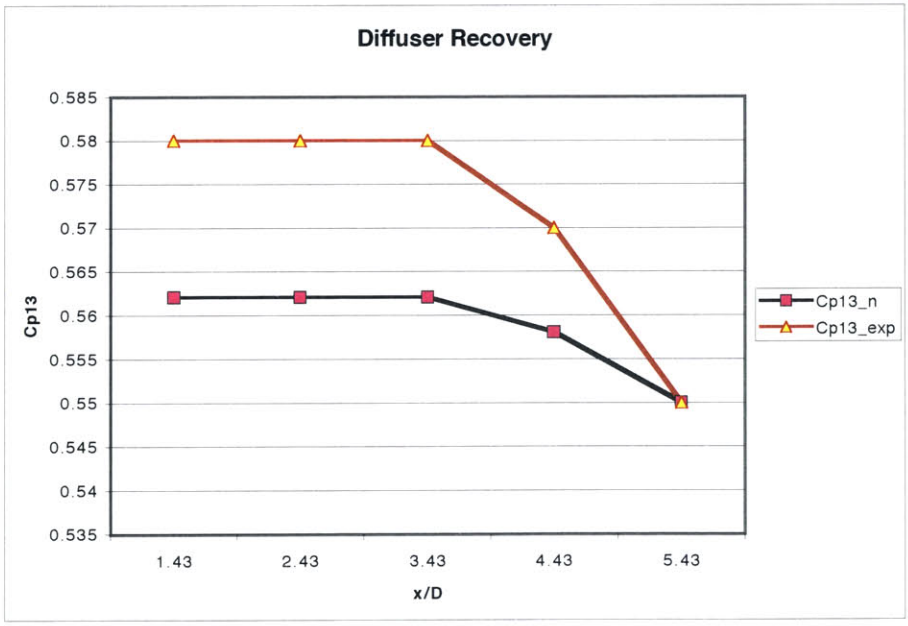

Figure 3-7: Overall Diffuser Static Pressure Recovery

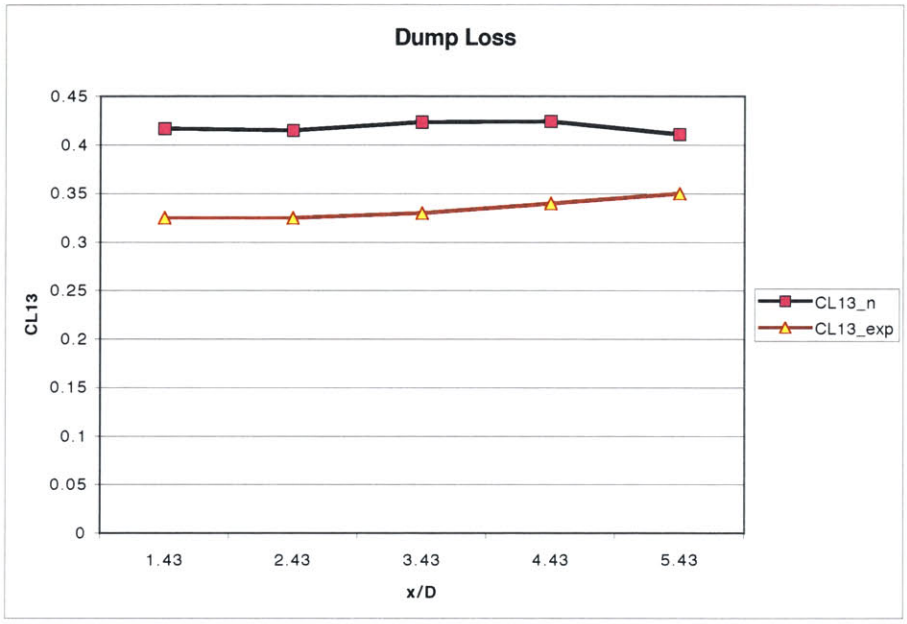

Figure 3-8: Overall Total Pressure Loss

Chapter 4

Turbulent Integral Shear Layer Model

In this chapter, the Turbulent Integral Shear Layer Model is proposed as an improvement over the algebraic model. First, the modeling assumptions are presented. Second, the governing equations for this turbulence model are derived and discretized. Finally, the results of this model are compared to those of the algebraic model and the experimental combustor/diffuser performance studies.

4.1 Theoretical Approach

In Chapter 3, the algebraic turbulence model accurately predicted the pre-diffuser and overall diffuser pressure recoveries as the dump gap length was varied. However, neither the general trend nor the absolute magnitudes of the dump loss were accurately predicted. The error in predicting the dump loss suggests that the mixing processes in the dump region and diffuser are not modeled accurately enough. In addition, this simple approach to quantifying the shear stress source terms is based on the experimental and theoretical results for simple free plane mixing layers and turbulent boundary layers, where some of the modeling assumptions, such as small velocity differences, negligible pressure gradients, and small streamwise curvature are incorrect in the dump region. The eddy viscosity model and the self-similar velocity profile both fail when these assumptions are no longer valid.

The spatial plane mixing layer does not grow symmetrically with respect to a horizontal centerline (Figure 4-1). It spreads into the low-speed stream and entrains fluid into it [8].

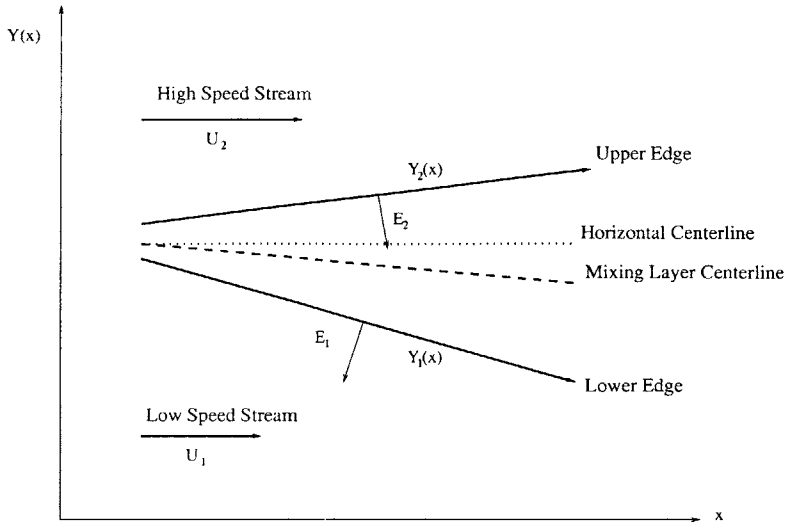

Figure 4-1: Plane Mixing Layer

In addition, the free stream velocities are not exactly parallel. Thus, there is mass and energy transport across a plane mixing layer that is not taken into account in the algebraic model.

The next step in improving the CFLOW turbulence model is to relax the relationship between the eddy viscosity and mixing layer thickness governed by Equation 3.3 and permit conduction and diffusion processes across the mixing layers in CFLOW. The turbulent viscosity hypothesis is still retained at this step, but the relationship between the Reynolds stress and the mean velocity gradient becomes a function of the flow conditions. Hence, the one-equation model of turbulence that is proposed in this chapter treats the eddy viscosity as an evolving quantity. Out of this new model comes a mechanism for conduction and diffusion processes which govern the behavior of the plane mixing layer.

4.1.1 Modeling Assumptions

The assumptions for the Turbulent Integral Shear Layer Model are:

1. The mixing layer is thin ($\frac{\delta_s}{L} \ll 1$).

2. The flow is highly turbulent ($\frac{\nu_t}{\nu} \gg 1$).

3. The eddy viscosity and the shear layer thickness are state variables; Prandtl's second hypothesis is relaxed.

4. Pressure gradients are negligible.

5. Streamline curvature effects are negligible.

6. Mass and energy transfer are not negligible across mixing layers.

7. Compressibility effects are negligible; the shear layer is incompressible.

4.1.2 Spalart-Allmaras Model

The Spalart-Allmaras (S-A) Equation [4] , an empirically-determined one-equation turbulence model for the eddy viscosity transport, is

$$\frac{D\nu_t}{Dt} = c_{b1}S\nu_t + \frac{1}{\sigma_t}[\nabla \cdot (\nu_t \nabla \nu_t) + c_{b2}(\nabla \nu_t)^2] \tag{4.1}$$

where $S \equiv \frac{1}{2}(\frac{\partial U_i}{\partial x_j} + \frac{\partial U_j}{\partial x_i})$ is the rate of strain tensor, σ_t is the turbulent Prandtl number, and c_{b1} and c_{b2} are empirically determined constants. They are calibrated for high Reynolds number free shear flows and boundary layers. The kinematic viscosity does not enter into the equation because "energy and information cascades flow only from the large scales to the small scales" [4].

Drela [3] integrated the steady S-A equation and the continuity equation for a compressible 2-D thin shear layer in order to produce an integral form of the S-A model. The steady S-A equation for a thin shear layer is

$$\rho u \frac{\partial \nu_t}{\partial x} + \rho v \frac{\partial \nu_t}{\partial y} = c_{b1}\rho \nu_t S + \frac{1}{\sigma_t}[\frac{\partial}{\partial y}(\rho \nu_t \frac{\partial \nu_t}{\partial y}) + c_{b2}\rho(\frac{\partial \nu_t}{\partial y})^2] \tag{4.2}$$

and the continuity equation for a steady, compressible flow in a thin, 2-D shear layer is

$$\frac{\partial(\rho u)}{\partial x} + \frac{\partial(\rho v)}{\partial y} = 0 \tag{4.3}$$

The axial velocity u, the radial velocity v, density ρ, and the eddy viscosity ν_t are defined to be time-averaged quantities. Integrating the continuity equation and the steady Spalart-Allmaras equation from the lower edge, Y_1, to the upper edge, Y_2 results in the integral form of the S-A Equation.

$$\int_{Y_1}^{Y_2} [\nu_t(\ 4.3) + (\ 4.1)]dy \tag{4.4}$$

$$\frac{d(\rho_e u_e \delta_\nu)}{dx} - c_{b1} P_\nu - c_{b2} D_\nu = \frac{1}{\sigma_t}[(\rho \nu_t \frac{\partial \nu_t}{\partial y})_1 - (\rho \nu_t \frac{\partial \nu_t}{\partial y})_2] + (\rho E \nu_t)_2 - (\rho E \nu_t)_1 \tag{4.5}$$

where the eddy viscosity thickness and the production and diffusion integrals are defined as:

$$\delta_\nu = \int_{Y_1}^{Y_2} \nu_t \frac{\rho u}{\rho_e u_e} dy \tag{4.6}$$

$$P_\nu = \int_{Y_1}^{Y_2} \rho \nu_t S dy \tag{4.7}$$

$$D_\nu = \int_{Y_1}^{Y_2} \rho (\frac{\partial \nu_t}{\partial y})^2 dy \tag{4.8}$$

The edge velocity, u_e, is an arbitrary quantity for free mixing layers. Unlike a boundary layer where the edge velocity is clearly the axial velocity component in the irrotational free stream, u_e is not readily identified for a plane mixing layer. In this analysis, $u_e \equiv \frac{1}{2}(U_1 + U_2)$, the average velocity of two adjacent streamtubes. The new term, the entrainment velocity E, is defined as

$$E = u \frac{dY}{dx} - v. \tag{4.9}$$

It is the velocity component normal to the edge of the mixing layer. The eddy viscosity thickness and the production and diffusion terms are approximated by assuming that there is no density variation within the mixing layer and that the velocity and eddy viscosity profiles are:

$$u(\frac{y}{\delta}) = \frac{1}{2}[U_1 + U_2 + (U_1 - U_2) cos(\pi \frac{y}{\delta})] \tag{4.10}$$

$$\nu_t(x, \frac{y}{\delta}) = \frac{\pi}{2} \nu_m(x) sin(\pi \frac{y}{\delta}) \tag{4.11}$$

These profiles contain properties consistent with the physical flow. The velocity gradient is zero at the edges and maximum at the centerline. The eddy viscosity is maximum at the centerline and zero at the edges.

Inserting these profiles and assumptions into the integral definitions yield:

$$\delta_\nu = K_N \nu_m \delta \tag{4.12}$$

$$P_\nu = K_P \rho \nu_m \Delta U \tag{4.13}$$

$$D_\nu = K_D \rho \frac{\nu_m^2}{\delta} \tag{4.14}$$

where $\Delta U \equiv U_2 - U_1$ for $U_2 > U_1$. Inserting these terms and noting that the eddy viscosity is zero at the edge of the mixing layer, the S-A Equation becomes

$$\frac{d(K_N u_e \nu_m \delta)}{dx} = c_{b1} K_P \nu_m \Delta U + \frac{c_{b2}}{\sigma_t} K_D \frac{\nu_m^2}{\delta} \tag{4.15}$$

4.1.3 Karman-Integral Momentum Equation

The free mixing layer form of the von Karman Integral Momentum Equation has been derived by Drela [3] in the following manner.

Start from the governing equations (continuity and x-momentum) in boundary layer form.

$$\frac{\partial(\rho u)}{\partial x} + \frac{\partial(\rho v)}{\partial y} = 0 \tag{4.16}$$

$$\rho u \frac{\partial u}{\partial x} + \rho v \frac{\partial u}{\partial y} = \rho_e u_e \frac{du_e}{dx} + \frac{\partial \tau}{\partial y} \tag{4.17}$$

where u_e is the edge velocity.

Integrate the sum of both equations over the mixing layer

$$\int_{Y_1}^{Y_2} [(u - u_e)(\ 4.16) + (\ 4.17)] dy \tag{4.18}$$

These steps result in the second governing equation of the turbulence model.

$$\frac{d(\rho_e u_e^2 \theta)}{dx} + \rho_e u_e \delta^* \frac{du_e}{dx} - \tau_1 + \tau_2 = \rho_2 E_2 (u_e - u_2) - \rho_1 E_1 (u_e - u_1) \tag{4.19}$$

E_1 and E_2 are the entrainment velocites at Y_1 and Y_2, respectively (see Figure 4-1).

The displacement and momentum thicknesses are defined by:

$$\delta^* = \int_{Y_1}^{Y_2} (1 - \frac{\rho u}{\rho_e u_e}) dy \tag{4.20}$$

$$\theta = \int_{Y_1}^{Y_2} (1 - \frac{u}{u_e}) \frac{\rho u}{\rho_e u_e} dy \tag{4.21}$$

The entrainment velocity, E, is an extra unknown in the system, which must be modeled. Prandtl [9] suggested that growth of a turbulent mixing layer was related to the fluctuating transverse velocity component via

$$\frac{D\delta}{Dt} \propto v'. \tag{4.22}$$

v' can be related to the Reynolds shear stress, $-\rho u'v'$, by

$$v' \propto u' \propto \sqrt{-u'v'}. \tag{4.23}$$

Thus, the shear layer growth can be related to the Reynolds stress.

$$\frac{D\delta}{Dt} = K_E\sqrt{-u'v'} \tag{4.24}$$

$$\frac{D\delta}{Dt} = K_E\sqrt{\frac{\tau_s}{\rho}} \tag{4.25}$$

K_E is the entrainment constant, which should be calibrated to a nominal value.

The net entrainment velocity into the shear layer will result in its growth. This entrainment of the outer fluid into the mixing layer takes place only when subject to Reynolds stresses. Thus the net entrainment velocity, E_n, is

$$E_n = K_E\sqrt{\frac{\tau_s}{\rho}} \tag{4.26}$$

Substituting the turbulent viscosity hypothesis for shear stress into (4.26) yields

$$E_n = K_E\sqrt{\frac{\nu_m(U_2 - U_1)}{\delta}} \tag{4.27}$$

Governing Equation

As previously stated, the edge velocity is defined to be the average velocity of the mixing layer. After substituting this definintion into the right hand side of Equation 4.19, the von Karman Integral Momentum Equation simplifies to

$$\frac{d(\rho_e u_e^2\theta)}{dx} + \rho_e u_e \delta^* \frac{du_e}{dx} - \tau_1 + \tau_2 = -\frac{1}{2}\rho(E_1 + E_2)\Delta U \tag{4.28}$$

In addition, the Reynolds stresses are negligible at the edges of the layer, which means that

$$\tau_1 = \tau_2 = 0 \tag{4.29}$$

For a constant density shear layer subject to the assumed velocity cosine profile, the displacement thickness is zero.

$$\delta^* = 0 \tag{4.30}$$

Also, the momentum thickness can be simplified to

$$\theta = f_\theta \delta \tag{4.31}$$

where f_θ is defined as:

$$f_\theta = -\frac{1}{8}\frac{\Delta U}{u_e} \tag{4.32}$$

A negative momentum thickness signifies that the shear layer is an excess of momentum instead of a defect of momentum. Combining these assumptions into the von Karman equation yields

$$\frac{d(u_e^2 f_\theta \delta)}{dx} = -\frac{1}{2}(E_1 + E_2)\Delta U \tag{4.33}$$

The net entrainment velocity is defined as

$$E_n = E_1 + E_2, \tag{4.34}$$

The observed linear growth of the classical turbulent plane mixing layer means that the net entrainment velocity is finite. The entire right-hand side of (4.33) and the $u_e f_\theta$ term on the left-hand side of (4.33) are constant for $\frac{du}{dx} = 0$. Thus, $\frac{d\delta}{dx} = constant$ confirms that there must be a net entrainment of fluid through the mixing layer in order to match the linear thickness growth.

By inserting Equation 4.34 and Equation 4.27 into Equation 4.33, the von Karman Integral Momentum Equation becomes

$$\frac{d(u_e^2 f_\theta \delta)}{dx} = -\frac{1}{2}K_E\sqrt{\frac{\nu_m \Delta U}{\delta}}\Delta U \tag{4.35}$$

4.1.4 Discretized Governing Equations

The integral turbulence model is calibrated to evolve as a classical plane mixing layer in the case where the axial velocities of the inviscid streams are constant and the radial velocities are zero. The eddy viscosity and the mixing layer thickness both grow linearly with x when the freestream velocities are constant. The S-A Equation is calibrated by placing calibration constant, K_c, on the right-hand side of Equation 4.15 and then solving for it. Substituting Equation 4.10 and Equation 4.11 into Equation 4.7 and Equation 4.8 yields $K_P = K_D$. After algebraic manipulation, the S-A Equation becomes

$$\frac{d(u_e \nu_m \delta)}{dx} = K_c(c_{b1}\nu_m \Delta U + \frac{c_{b2}}{\sigma_t}\frac{\nu_m^2}{\delta}) \tag{4.36}$$

$$K_c = \frac{2K_\delta}{c_{b1} + \frac{c_{b2}}{\sigma_t}K_\nu} \tag{4.37}$$

K_c is only a function of empirical constants, and, therefore, is a constant as well.

The von Karman Equation was calibrated in order to solve for the appropriate value of K_E, which is unknown otherwise. Substituting Equation 3.6 and Equation 3.7 into Equation 4.35 yields

$$K_E = \frac{1}{4}\frac{K_\delta}{K_\nu^{0.5}}\frac{\Delta U}{u_e}. \tag{4.38}$$

K_E and f_θ are not constants but functions of the velocity field. In CFLOW, however, they are calibrated based on the maximum velocity difference at the pre-diffuser inlet. Based on these procedures, the linear growth rates of ν_m and δ are recovered when the axial velocities are constant, and there are no radial components.

After this calibration procedure, the governing equations are discretized, linearized, and then implemented in CFLOW.

$$(u_{ave_1}\nu_{T1}\delta_{T1} - u_{ave_0}\nu_{T0}\delta_{T0}) = C_1(\Delta u_{T0}\nu_{T0} + \Delta u_{T1}\nu_{T1})\Delta x + C_2(\frac{\nu_{T0}^2}{\delta_{T0}} + \frac{\nu_{T1}^2}{\delta_{T1}})\Delta x \tag{4.39}$$

$$f_\theta(u_{ave_1}^2\delta_{T1} - u_{ave_0}^2\delta_{T0}) = C_3(\frac{\Delta u_{T0}^{1.5}\nu_{T0}^{0.5}}{\delta_{T0}^{0.5}} + \frac{\Delta u_{T1}^{1.5}\nu_{T1}^{0.5}}{\delta_{T1}^{0.5}})\Delta x \tag{4.40}$$

$$C_1 = \frac{1}{2}K_c c_{b1} \tag{4.41}$$

$$C_2 = \frac{1}{2}K_c\frac{c_{b2}}{\sigma_t} \tag{4.42}$$

$$C_3 = \frac{1}{4} K_E \tag{4.43}$$

$$u_{ave} = \frac{1}{2}(U_1 + U_2) \tag{4.44}$$

4.1.5 Source Terms

Mass Transfer

The mass transport across streamsurface area, A_s, is

$$\tilde{M} = \rho E_n A_s \tag{4.45}$$

where $\tilde{M}$ is the mass flow source term in the Conservation of Mass (see Chapter 2). Thus, increasing the velocity difference raises the shear stress, which results in a greater net entrainment of fluid into the low-speed stream.

Momentum Transfer

The Reynolds shear stress is governed by

$$\tau_s = \rho \nu_m \frac{\Delta U}{\delta} \tag{4.46}$$

which must be resolved into the axial and radial directions. Respectively, the expressions for the momentum transfer source terms (see Chapter 2), S_x and S_r, are

$$S_x = \tau_s A_s \hat{x} \tag{4.47}$$

$$S_r = \tau_s A_s \hat{r} \tag{4.48}$$

The convective momentum transfer source terms are defined in the following manner.

$$S_{cx} = -\rho E_n u A_s \hat{x} \tag{4.49}$$

$$S_{cr} = -\rho E_n v A_s \hat{r} \tag{4.50}$$

Energy Transfer

The energy transfer source terms in the Conservation of Energy (Chapter 2) are finite in the integral turbulence model. The heat transfer rate source term, H_s is finite only in the burner region. For the studies conducted in Chapters 3 and 4, this term is set to zero.

$$H_s = 0 \tag{4.51}$$

The enthalpy flux term, H_{tx} is defined as:

$$H_{tx} = \tilde{M} h_T \tag{4.52}$$

where $\tilde{M}$ is the mass transport across the cell edges and h_T is the total enthalpy of the high speed stream.

The work transfer term, W_s, is

$$W_s = \tau_s u_e \tag{4.53}$$

Flow Tangency

The flow tangency condition is updated in order to account for the entrainment component of velocity across the control volume edges. The net entrainment velocity contributes a radial component of velocity.

$$u\frac{dr}{dx} - v = E_n \tag{4.54}$$

Turbulence Model Boundary Conditions

Additional boundary conditions are necessary due to the increased size of the system of governing equations. Inlet values of the eddy viscosity, the mixing layer thickness, and the turbulent length scale, $\hat{L_{turb}}$, are prescribed based on the expressions (see Appendix B) shown below,

$$\hat{\delta} = 1 \tag{4.55}$$

$$\hat{\nu_t} = (\nu_t/\nu)\frac{M}{Re_{\delta_o}} \tag{4.56}$$

$$\hat{L_{turb}} = \frac{Re_L}{Re_{\delta_o}} \tag{4.57}$$

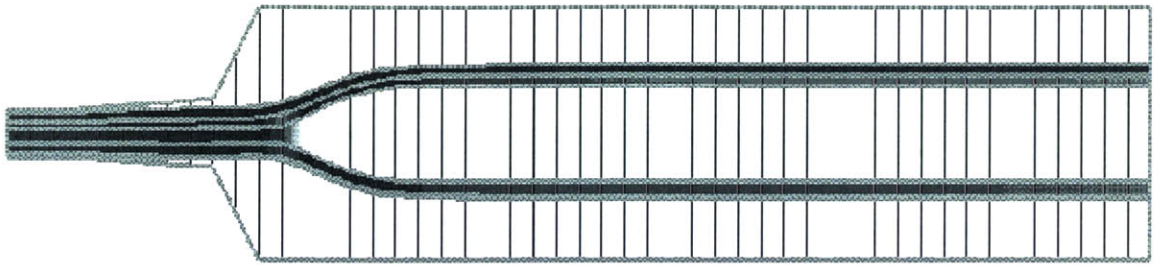

Figure 4-2: Flow Plot: Mach Number

where Re_L is the Reynolds number based on the length scale of the mean flow, Re_{δ_o} is the Reynolds number based on the inlet mixing layer thickness, and M is the mean inlet Mach number. In CFLOW, $(\nu_t/\nu) = 10^2$ and $Re_{\delta_o} = 10^4$, which are ballpark values for turbulent mixing layers.

4.2 Results

The results of the Turbulent Integral Shear Layer Model applied to the Lohmann study do not yield physically accurate solutions in CFLOW at the calibration point ($x_d/D = 1.43$). As Figure 4-2 shows, the high speed flow emanating from the pre-diffuser hugs the burner walls, which leaves two large low-speed streamtubes adjacent to the diffuser walls. A sufficient amount of turbulent mixing would cause the high speed streams to decrease in velocity and the low speed streams to increase in velocity. According to continuity, a concomitant effect is for the streamtube areas to increase in the high speed streams as their velocities decrease. Similarly, the flow-through areas for the low speed streams decrease as their velocities increase. This effect results in the closure of the recirculation zones. However, Figure 4-4 shows that there is insufficient mixing in the dump region to close the recirculation zones in this case. Figure 4-3 demonstrates that all of the pressure recovery occurs in the pre-diffuser. The small pressure recovery provided by the diffuser is a direct result of the low amount of turbulent mixing in the dump region and along the diffuser flow paths. Further analysis of results from the integral model show that the eddy viscosity decreases and the mixing layer thickness grows rapidly as the flow leaves the pre-diffuser

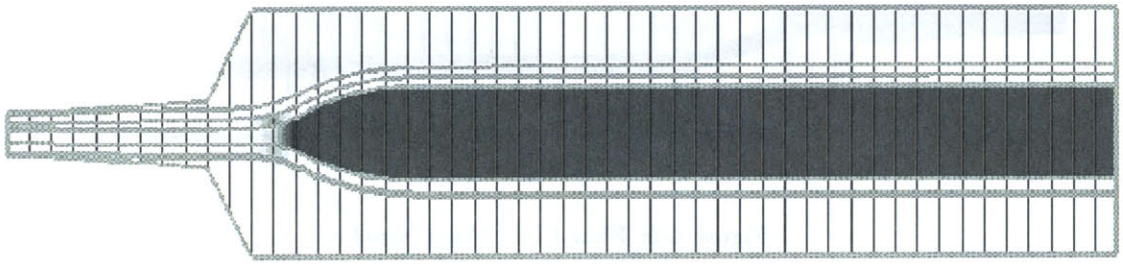

Figure 4-3: Flow Plot: Static Pressure Recovery

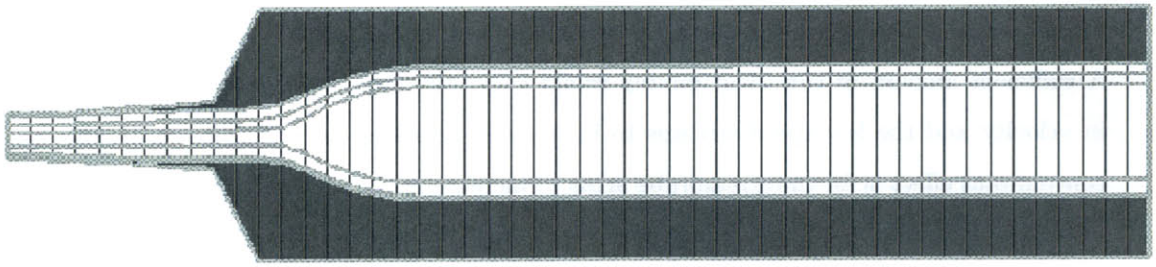

Figure 4-4: Flow Plot: Total Pressure Loss

and enters the dump region. This combined effect produces values of the shear stress that are 3 to 4 orders of magnitude smaller those given in the algebraic model, which results in low values of Reynolds shear stress (compared to the momentum flux) predicted by Equation 4.46. In order to demonstrate the dramatic effects of sufficient mixing in the dump region, Equation 4.46 has been amended with the mixing coefficient C_τ. Setting $C_\tau = 10^3$ offsets the low values of $\frac{\nu_m}{\delta}$ that have been previously described.

$$\tau_s = C_\tau \rho \nu_m \frac{\Delta U}{\delta} \tag{4.58}$$

4.2.1 Flow Plots

The following flow plots show the CFLOW results from the Lohmann case at the calibration point, where $x_d/D = 1.43$, $C_\tau = 10^3$, and $C_f = 0.02$.

Mach Number ($C_\tau = 10^3$)

As shown in Figure 4-5, the Reynolds shear stresses are high enough to close the recirculation zones and properly mix out the flow downstream of the dump region. The increase in flow area and the turbulent mixing processes decreases the Mach number as the flow travels downstream.

Static Pressure Recovery ($C_\tau = 10^3$)

Figure 4-6 shows that the most of the static pressure recovery occurs in the pre-diffuser. In addition, the radial pressure distribution at the combustor exit is uniform.

Total Pressure Loss ($C_\tau = 10^3$)

Figure 4-7 illustrates the increase in C_L in the dump region and downstream of the burner front end at a result of turbulent mixing. Momentum transfer between among the streamtubes in the ID and OD flow paths change the values of C_L as the flow moves downstream. As a result, the core streams, which have lower levels of total pressure loss than the recirculation zone streamtubes, have increasing levels of C_L further downstream.

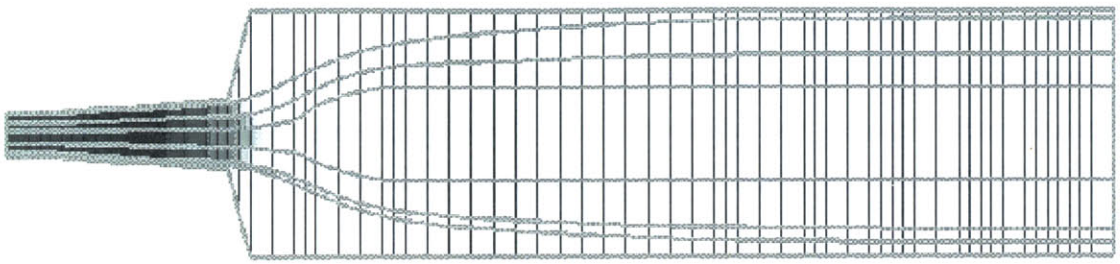

Figure 4-5: Flow Plot: Mach number ($C_\tau = 10^3$)

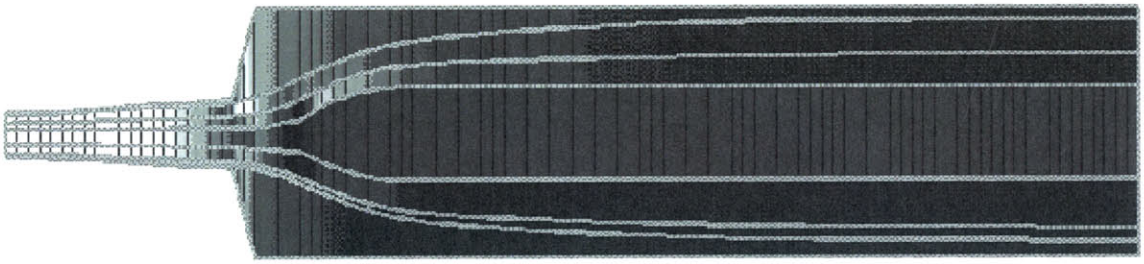

Figure 4-6: Flow Plot: Pressure Recovery ($C_\tau = 10^3$)

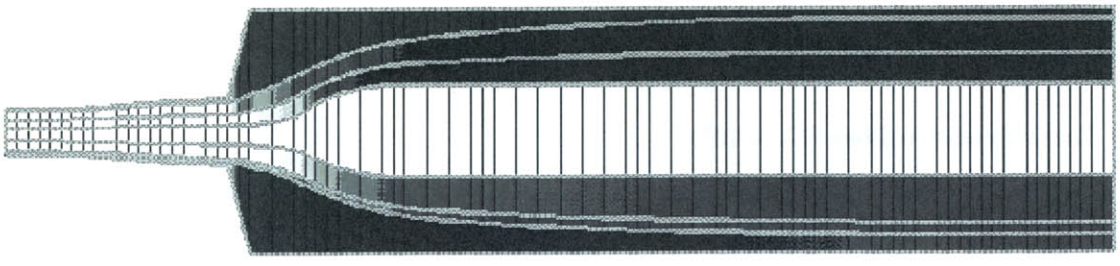

Figure 4-7: Flow Plot: Total Pressure Loss ($C_\tau = 10^3$)

4.2.2 Validation

Following the calibration procedure in the previous section, a parametric study was performed in order to compare the results of the integral model at $C_\tau = 10^3$ with those of the algebraic model and with experimental data from the Lohmann study. 'nt' denotes the CFLOW performance metrics for the integral model.

Pre-Diffuser Static Pressure Recovery

Figure 4-8 demonstrates that the pre-diffuser static pressure recovery for $C_\tau = 10^3$ matches the experimental data; the amended integral model curve overlaps the experimental data curve.

Overall Diffuser Static Pressure Recovery

As shown in Figure 4-9, the amended model does not match the trend nor the absolute magnitudes for the experimental value of $C_{p_{13}}$. As x_d/D increases, the pressure recovery increases when it should decrease. In addition, the pressure recovery is underpredicted by a maximum of 9 percent.

Overall Total Pressure Loss

The dump loss slightly decreases as the dump gap length increases (Figure 4-10). Also, the magnitude of the $C_{L_{13}}$ overpredicted by the amended integral model by 45 percent.

4.3 Discussion

These results show that the amended integral model does not capture the mixing processes downstream of the pre-diffuser exit plane accurately. Simply increasing the value of C_τ alone does not offset the modeling errors that possibly result from inaccurate choices of the inlet boundary conditions for the turbulence model. The ability to decrease Re_{δ_o} to 10^3 or increase ν_t/ν to 10^3 in CFLOW will decrease the growth of the mixing layer thickness and increase the magnitude of the eddy viscosity in the pre-diffuser and dump regions. However, the integral model cannot be solved under these conditions. The high nonlinearity of this system may be a deterrent in achieving a reasonable solution using the current numerical approach.

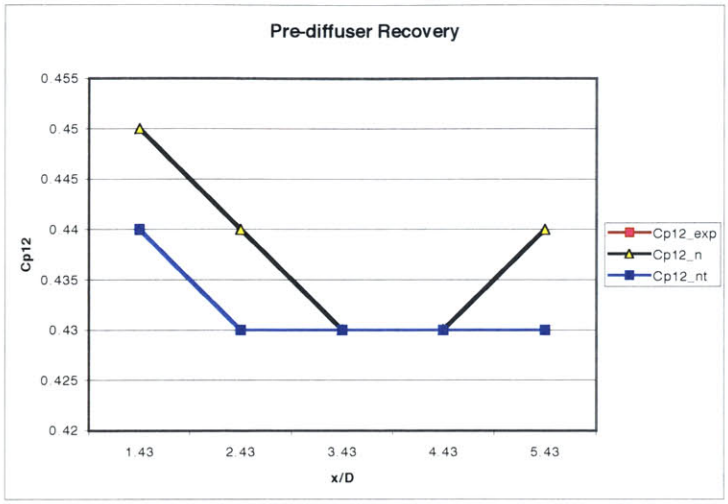

Figure 4-8: Pre-diffuser Static Pressure Recovery ($C_\tau = 10^3$)

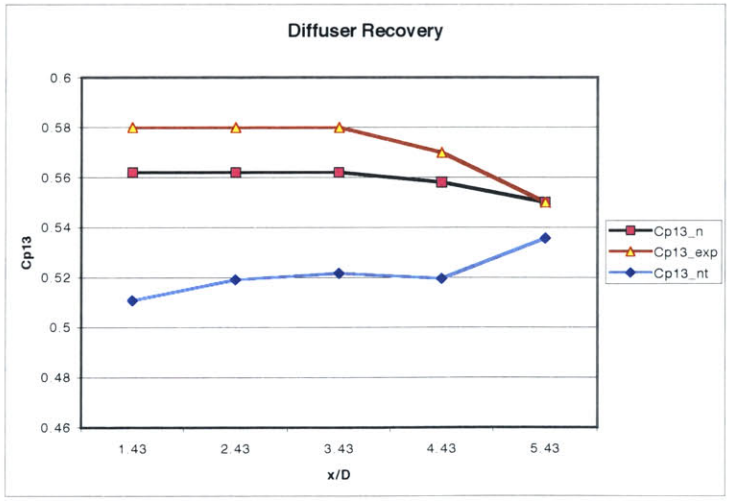

Figure 4-9: Overall Diffuser Static Pressure Recovery ($C_\tau = 10^3$)

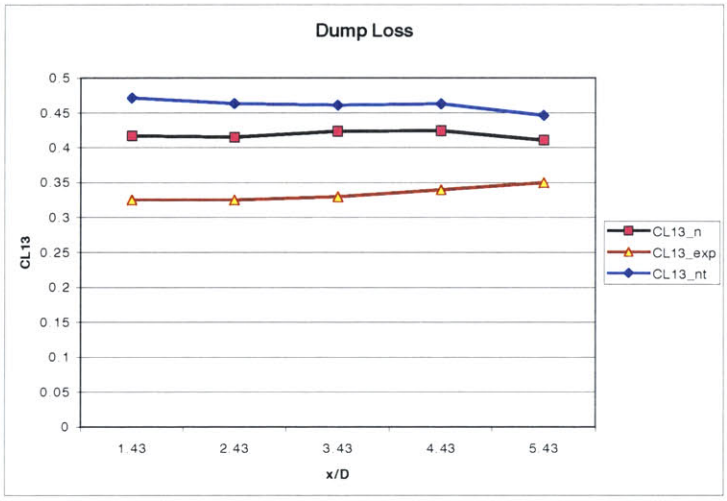

Figure 4-10: Overall Total Pressure Loss ($C_\tau = 10^3$)

Chapter 5

Summary and Future Work

5.1 Summary

A physics-based, reduced-order computational flow model for combustors has been developed. CFLOW models flows through combustors using multiple compressible and inviscid streamtubes where the plane mixing layer is used as the mechanism for mass, momentum, and energy transfer via turbulent mixing. Two turbulence models have been developed which quantify these source terms.

The Algebraic Turbulent Shear Layer Model assumes that the eddy viscosity is constant across the plane mixing layer and is related to the thickness via Prandtl's second hypothesis. Using this approach, an expression for the turbulent shear stress that only depends on the velocity difference squared across the shear layer is derived. Conduction and diffusion processes across the mixing layer are assumed to be negligible. The validation studies demonstrate that this model accurately predicts the pre-diffuser and overall diffuser pressure recoveries. CFLOW predicts the behavior of the dump loss as the dump gap changes. However, the magnitude of the dump loss is 30 percent greater in CFLOW than was measured in the Lohmann study.

The Turbulent Integral Shear Layer Model assumes that the eddy viscosity varies sinusoidally across the plane mixing layer and that the mean quantity is a variable in CFLOW. The Spalart-Allmaras model and the von Karman Integral Equation comprise the integral model. The conduction and diffusion processes naturally come out of this turbulence model. The level of turbulent mixing in the dump region is 3 to 4 orders of magnitude lower than predicted by the algebraic model. A high speed jet hugs the burner tightly and does not mix

out. This insufficient amount of turbulent mixing does not allow the recirculation zones in CFLOW to close as they should. Thus, the flow predicted by using this turbulence model is unphysical. Increasing the magnitudes of the Reynolds shear stresses through a mixing constant results in the closure of the recirculation zones. However, the trend studies in Section 4.2 show that the flow physics in the regions downstream of the pre-diffuser exit plane are not accurately represented by the amended integral model. These modeling errors are due, in part, to CFLOW's inability to solve the flow for lower values of Re_{δ_o} and higher values of (ν_t/ν).

5.2 Future Work

There are several features that require further development in order for CFLOW to accurately predict combustor performance. A more robust numerical scheme should be implemented in order to solve the flow for more reasonable initial conditions. In addition, some of the basic features that should be implemented in order to arrive at a more complete combustor model include streamwise curvature effects, the effects of dilution holes, a heat release model, and blockage effects.

5.2.1 Augmented Newton Solver

The high nonlinearity of the Integral Turbulence Model's governing equations prevent them from being solved for reasonable initial guesses of the state vector. An improved version of CFLOW's Newton solver may permit solutions using initial conditions based on $Re_{\delta_o} < 10^4$ and $(\nu_t/\nu) > 10^2$. As a result, the eddy viscosity may grow, instead of decrease, in the pre-diffuser and dump regions, and the Reynolds stresses will increase enough to cause sufficient levels of turbulent mixing.

5.2.2 Streamline Curvature

Mixing layers are strongly affected by streamline curvature [1]. Strong curvature causes either an increase or decrease in the turbulence levels. These effects can be captured by adding a rotation function to the production term in the Spalart-Allmaras turbulence model [21].

5.2.3 Dilution Hole Modeling

A dilution hole model for CFLOW should be one in which the dilution jet angle, the jet velocity, and the discharge coefficient are functions of the pressure field. Thus, the sensitivity of dilution air mass flow and jet angle to combustor mass flow split or back pressure can be quantified. A good approach involves the use of empirical relationships for the aforementioned quantities outlined in a paper by Adkins and Gueroui [18].

5.2.4 Heat Release and Emissions Models

A CFLOW heat release model would be a function of pressure, temperature, and equivalence ratio. The sensitivity of combustor temperature rise to pressure and equivalence ratio changes may be useful to study. In addition, an emissions model would enable the prediction of NOx, Carbon Monoxide, unburned hydrocarbons, and other emissions. For example, Kerrebrock [19] discusses the correlation between NOx production and combustor inlet temperature.

5.2.5 Blockage Effects

Physical causes of blockage are not currently represented in CFLOW. For example, the struts for the fuel lines are flow obstructions. They affect the mass flow split and total pressure losses in combustors. Models for the mass flow defect and momentum drag induced by the presence of blockage-causing apparati should be included.

Appendix A

CFLOW User's Manual

This appendix contains the CFLOW user's manual. In order to run CFLOW, type the following commands followed by the casename.

1. **XPATHGEN**: This file generates the geometry. First, XPATHGEN prompts the user to enter number of axial control volume cells. Then, XPATHGEN asks the user to input the location of the 'blockage streams relative to the pre-diffuser walls.' The blockage streams are streamtubes 1, 2, 6, and 7. This routine stores this data in ***casename.ipd*** .

2. **FLOWGEN**: The file generates the initial condition for the flow field state vector. FLOWGEN prompts the user to enter the Mach number of the core flow, the Mach numbers of the blockage streams, the mass flow split, the ratio of specific heats, the mixing layer constant, K_t, and the wall friction coefficient, C_f. This routine stores this data in ***casename.ifd*** .

3. **CFLOW**: CFLOW reads in the information stored in the ***.ifd*** and ***.ipd*** files. Then it solves the governing equations and satisfies all of the matching conditions. Finally, it creates two output files: ***casename.opd*** and ***casename.ofd*** .

4. **CVIZ**: CVIZ plots the CFLOW results stored in the ***.ofd*** and ***opd*** files using Visual3.

Appendix B

Dimensional Analysis

The inlet state variables and thermodynamic constants are non-dimensionalized in the following manner, where 'o' denotes a reference quantity.

$$\hat{a} = \frac{a}{U_o} \tag{B.1}$$

$$\hat{u} = \frac{u}{U_o} \tag{B.2}$$

$$\hat{v} = 0 \tag{B.3}$$

$$\hat{\rho} = \frac{\rho}{\rho_o} \tag{B.4}$$

$$\hat{C_p} = \frac{C_p}{C_{po}} \tag{B.5}$$

$$\hat{R} = \frac{R}{C_{po}} \tag{B.6}$$

$$\hat{T} = \frac{C_p T}{U_o^2} \tag{B.7}$$

$$\hat{p} = \frac{p}{\rho_o a_o^2} \tag{B.8}$$

$$\hat{\delta} = \frac{\delta}{L_o} \tag{B.9}$$

$$\hat{\nu} = \frac{\nu}{U_o L_o} \tag{B.10}$$

$$\hat{L} = \frac{L}{L_o} \tag{B.11}$$

Currently in CFLOW, the reference velocity, U_o is set equal to the static speed of sound, a_o, and the reference length, L_o, is equal to the inlet duct height, D_o. (Note that v is zero due to the uniform flow condition at the inlet.) Subsituting these definitions into the expressions above yields the following.

$$\hat{a} = 1 \tag{B.12}$$

$$\hat{u} = M \tag{B.13}$$

$$\hat{v} = 0 \tag{B.14}$$

$$\hat{\rho} = 1 \tag{B.15}$$

$$\hat{C_p} = 1 \tag{B.16}$$

$$\hat{R} = \frac{\gamma - 1}{\gamma} \tag{B.17}$$

$$\hat{T} = \frac{1}{\gamma - 1} \tag{B.18}$$

$$\hat{p} = \frac{1}{\gamma} \tag{B.19}$$

$$\hat{\delta} = 1 \tag{B.20}$$

$$\hat{\nu_t} = \frac{\nu_t}{U_o \delta_o} \tag{B.21}$$

$$\hat{L_{turb}} = \frac{L}{\delta_o} \tag{B.22}$$

$$\hat{L_{mean}} = \frac{L}{D_o} \tag{B.23}$$

M is the inlet Mach number. $\hat{L_{mean}}$ is the length scale of the mean flow, and $\hat{L_{turb}}$ is the length scale of the dynamic turbulence model.

The nondimensional forms of $\hat{\nu_t}$ and $\hat{L}$ are the following.

$$\hat{\nu_t} = (\nu_t/\nu)\frac{M}{Re_{\delta_o}} \tag{B.24}$$

$$\hat{L_{turb}} = \frac{Re_L}{Re_{\delta_o}} \tag{B.25}$$

$(\nu_t/\nu) = 10^2$ and $Re_{\delta_o} = 10^4$, which are ballpark values for turbulent mixing layers.

Appendix C

Plane Mixing Layer Growth

The linear growth rate of a free mixing layer can be derived from dimensional analysis in the following manner.

Start with the continuity equation for an steady, incompressible, thin shear layer.

$$\frac{\partial u}{\partial x} + \frac{\partial v}{\partial y} = 0 \tag{C.1}$$

The axial component of the Navier-Stokes equations for an steady, incompressible, thin shear layer which is not under the influence of any pressure gradients is

$$v\frac{\partial u}{\partial y} = \frac{1}{\rho}\frac{\partial \tau}{\partial y} \tag{C.2}$$

The shear stress is computed using the turbulent viscosity hypothesis.

$$\tau = \rho(\nu + \nu_t)\frac{\partial u}{\partial y} \tag{C.3}$$

The flow is assumed to be turbulent, where

$$\frac{\nu_t}{\nu} \gg 1 \tag{C.4}$$

Thus, the approximate expression for the turbulent shear stress is

$$\tau \approx \rho\nu_t\frac{\partial u}{\partial y} \tag{C.5}$$

Substituting this expression into the x-momentum equation is

$$v\frac{\partial u}{\partial y} = \nu_t \frac{\partial^2 u}{\partial y^2} \tag{C.6}$$

where the eddy viscosity is constant across the mixing layer. Prandtl's second hypothesis specifies the relationship between the eddy viscosity, the velocity difference across the mixing layer, and the thickness of the layer.

$$\nu_t = K_\nu \Delta U \delta \tag{C.7}$$

Applying dimensional analysis to the continuity and momentum equations, the following relationships are valid.

$$v \sim \bar{U}\frac{\delta}{L} \tag{C.8}$$

$$\frac{vU}{\delta} \sim \nu_t \frac{\bar{U}}{\delta^2} \tag{C.9}$$

where $\bar{U}$ is the average velocity in the shear layer and L is the characteristic length. Inserting the expression for v and the equation for eddy viscosity into the momentum equation yields the following.

$$\frac{\bar{U}^2}{L} \sim K_\nu \frac{\Delta U \bar{U} \delta}{\delta^2} \tag{C.10}$$

$$\frac{\bar{U}}{L} \sim K_\nu \frac{\Delta U}{\delta} \tag{C.11}$$

$$\delta \sim K_\nu \frac{\Delta U}{\bar{U}} L \tag{C.12}$$

Thus, for the case of two uniform streams with no velocity gradients, the mixing layer thickness grows linearly.

$$\delta(L) = (constant)L \tag{C.13}$$

Bibliography

[1] Frank M. White. *Viscous Fluid Flow.* McGraw-Hill Series in Mechanical Engineering.

[2] David Scott Underwood. *Primary Zone Modeling for Gas Turbine Combustors.* MIT Ph.D. Thesis., Cambridge, MA, 1999.

[3] Mark Drela. *Integral Boundary Layer Method with a One-Equation Turbulence Model.* Cambridge, MA 1994.

[4] P.R. Spalart and S.R. Allmaras. *A One-Equation Turbulence Model for Aerodynamic Flows.* AIAA-92-0439., Boeing Commercial Airplane Group., Seattle, WA

[5] Arthur H. Lefebvre. *Gas Turbine Combustion, Second Edition.* Taylor Francis., 1999

[6] D.P. Bertsekas. *Nonlinear Programming.* Athena Scientific, Belmont, MA, 1995

[7] John J. Bertin, Michael L. Smith. *Aerodynamics for Engineers.* Prentice Hall., Upper Saddle River, New Jersey 1998

[8] Stephen B. Pope. *Turbulent Flows.* Cambridge University Press., Cambridge, U.K., 2000

[9] L. Prandtl. *The mechanics of viscous fluids.* In W.F. Durand(ed.): Aerodynamic Theory, III, 16-208 (1935)

[10] R. Srinivasan, G. Freeman, J. Grahmann, E. Coleman. *Parametric Evaluation of the Aerodynamic Performance of an Annular Combustor-Diffuser System.* AIAA-90-2163. Allied-Signal Aerospace Company, Garrett Engine Division.,Phoenix, Arizona, 1990.

[11] Paul Nicholson, Aleksandra Mozdzanowska, David Darmofal. *Parametric Study of the Effect of Geometric Variations on Flow Fields in Combustors.* 16.62x Final Report. Massachusetts Institute of Technology, Cambridge, MA., 2001.

[12] R.P. Lohmann, R.J. Mador, M. Klein. *Diffuser/Combustor Interaction Studies in Annular Dump Diffuser/Burner Systems:Part I.* Pratt Whitney Aircraft., East Hartford, Connecticut., 1976.

[13] J.C. Hermanson, P.E. Dimotakis. *Effects of Heat Release in a Turbulent, Reacting Shear Layer.* Journal of Fluid Mechanics, Vol. 199, Feb. 1989, pp.333-375.

[14] J.K. Eaton and J.P. Johnston. *A Review of Research On Subsonic Turbulent-Flow Reattachment.* Department of Mechanical Engineering, Stanford University, Stanford, California 94305.

[15] J.K. Eaton and J.P. Johnston. *Turbulent Flow Reattachment: An Experimental Study of the Flow and Structure Behind a Backward-Facing Step.* Department of Mechanical Engineering, Stanford University, Stanford, California, 1980.

[16] S. Baker. *Regions of Recirculating Flow Associated with Two-Dimensional Steps.* Ph.D Thesis, Dept. of Civil Engineering, University of Surrey, 1997.

[17] M. McGuinness. *Flow with a Separation Bubble - Steady and Unsteady Aspects.* Ph.D. dissertation, Cambridge University, 1978.

[18] R. C. Adkins and D. Gueroui. *An Improved Method for Accurate Prediction of Mass Flows Through Combustor Liner Holes.* Journal of Engineering for Gas Turbines and Power, Vol. 108, 1986.

[19] Jack L. Kerrebrock. *Aircraft Engines and Gas Turbines.* Second Edition. The MIT Press, Cambridge, Massachusetts, 1992.

[20] F. H. Clauser. *Turbulent Boundary Layers in Adverse Pressure Gradients* J. Aeronautic. Sci., vol. 21, pp. 91-108.

[21] P. R. Spalart and M. Shur. *On The Sensitization of Turbulence Models to Rotation and Curvature* Boeing Commercial Airplane Group, Seattle, Washington.

3231-7